Biofabrication

PAPER

3D printing of step-gradient nanocomposite hydrogels for controlled cell migration

RECEIVED
25 March 2019

REVISED
3 July 2019

ACCEPTED FOR PUBLICATION
25 July 2019

PUBLISHED
22 August 2019

Andisheh Motealleh[1,10], **Betül Çelebi-Saltik**[2,3,10], **Nihal Ermis**[1,4], **Sacha Nowak**[5], **Ali Khademhosseini**[6,7,8,9] **and Nermin Seda Kehr**[1]

[1] Physikalisches Institut and Center for Soft Nanoscience, Westfälische Wilhelms-Universität Münster, Busse-Peus-Strasse 10, 48149 Münster, Germany
[2] Department of Stem Cell Sciences, Hacettepe University Graduate School of Health Sciences, Ankara, Turkey
[3] Center for Stem Cell Research and Development, Hacettepe University, Ankara, Turkey
[4] Chemistry Department Ondokuz Mayis University Körfez Mahallesi, 55270 Samsun, Turkey
[5] MEET—Electrochemical Energy Technology Corrensstraße 46, 48149, Münster, Germany
[6] Department of Bioengineering, University of California-Los Angeles, Los Angeles, CA, United States of America
[7] Department of Radiology, David Geffen School of Medicine, University of California-Los Angeles, Los Angeles, CA, United States of America
[8] Center for Minimally Invasive Therapeutics (C-MIT), University of California-Los Angeles, Los Angeles, CA, United States of America
[9] California NanoSystems Institute (CNSI), University of California-Los Angeles, Los Angeles, CA, United States of America
[10] Both authors contributed equally to this study.

E-mail: seda@uni.muenster.de

Keywords: 3d printing, gradient, nanocomposite hydrogel, cell migration, cell differentiation

Supplementary material for this article is available online

Abstract

In this study, we report the step-gradient nanocomposite (NC) hydrogel generated easily by spatial connection of different nanocomposite hydrogel pastes varying in the concentrations of nanomaterials with the aid of a 3D printing technique. The prepared 3D printed gradient NC hydrogel has self-adhesive properties and is used to direct the migration of fibroblast cells towards the higher concentration of biopolymer-coated silica-based nanomaterials (NMs) within the 3D network of the hydrogel. Furthermore, we demonstrate the potential application of our gradient NC hydrogel in migration and subsequent enhanced osteogenic differentiation of human bone marrow derived mesenchymal stem cells (hBM MSC). The osteogenic differentiation of hBM MSC is achieved in the absence of osteogenic differentiation medium due to the silica-based NMs. The increase in the NM content in the gradient construct promotes hBM MSC migration and results in higher Ca^{2+} deposition.

1. Introduction

The extracellular matrix (ECM), a three-dimensional (3D) nanofibrous network supports and regulates cell behavior (proliferation, differentiation and migration) by providing biochemical and mechanical signaling cues in a gradient manner [1, 2]. Cells migrate in the ECM towards the gradually increasing concentration of soluble signal factors and the ligands of the ECM during a wound healing process. Furthermore, gradient structures are present in and between the tissues, such as bone, skin, and cartilage. Therefore, biomaterials with mechanical and chemical gradients have been engineered to influence cell migration, proliferation and differentiation to regenerate tissues and tissue interfaces [3–5]. Gradients are also particularly important for the migration of stem cells [6, 7], not only for embryonic development, but also to mediate tissue repair and regeneration [8]. Stem cell migration plays an important role in the inhibition of the development of cancer or inflammatory diseases [8]. Therefore, control of the stem cell migration should be potentially used in cancer and other disease treatments and in improved cell therapy. Besides having chemical and mechanical gradient properties, engineered materials must also be fabricated with well-defined structures that can mimic native tissues' 3D anatomic geometries and inherent tissue cellular distributions to study and understand cell-material interactions properly.

In this respect there is interest in generating 3D (bio)printed biomaterials with biochemical and mechanical gradient properties to mimic the ECM and 3D anatomical geometries of the target tissue for tissue regeneration applications [9, 10]. The 3D printing technique [11, 12] can be used to fabricate biomaterials or cell-laden biomaterials, layer by layer, via computer-designed instructions into well-defined 3D structures to generate tissue-like constructions. For example, Moroni and his coworkers described surface energy and stiffness gradients in additive manufactured scaffolds for osteochondral regeneration [13]. Gurkan *et al* reported a biochemical gradient by bioprinting nanoliter droplets to mimic the native fibrocartilage phase [14]. In another study, Annabi and Khademhosseini demonstrated the fabrication of 3D-bioprinted gradient bone-like tissue constructs containing a perfusable vascular lumen [15]. Recently, Cross *et al* reported gradient nanocomposite hydrogels composed of Laponite-reinforced gelatin methacryloyl and methacrylated kappa carrageenan for interface tissue regeneration [16].

In tissue engineering, nanocomposite (NC) hydrogels have been used as better alternative biomaterials to hydrogels due to their improved mechanical, stimuli responsive, viscoelastic, hydrophilic and biocompatible properties that can mimic the native ECM environment and tissue structure [17–19]. NC hydrogels are generated by the incorporation of nanomaterials (NMs) as fillers into the hydrogel's matrix. Yet, despite their promising applications in tissue engineering and biomedicine, very few studies have investigated the potential of NC hydrogels [17–21] in 3D printing. In the few studies [22–26] demonstrated, 3D printed silver nanoparticles embedded a hydrogel matrix for the fabrication of a bionic ear [22], poly (ethyleneglycol)-diacrylate(PEGDA)/nanocrystalline hydroxylapatite NC hydrogels were used for osteochondral tissue regeneration [23] and polydiacetylene nanoparticles intercorporated PEGDA hydrogels to generate a liver-inspired 3D detoxification device [24]. In other interesting studies, Gaharwar *et al* reported Laponite nanosilicate reinforced kappa carrageenan (κCA) and the combination of κCA and gelatin methacryloyl (GelMA) nanocomposites as mechanically stiff and elastomeric bioinks for 3D bioprinting [25, 26]. Despite the promising applications of NC hydrogels in tissue engineering and biomedicine, the utilization of NC hydrogels in 3D printing of gradient biomaterial constructions for controlled cell migration needs to be investigated.

In this context, we describe the fabrication of a 3D printed step-gradient NC hydrogel with the main purpose of directing cell migration towards the higher concentration of biopolymer-coated NMs. We used poly-*D*-Lysine (PDL) to coat periodic mesoporous organosilica nanomaterials (PMOs) to obtain biopolymer-coated silica-based NMs. The PDL-coated PMOs were inserted into alginate hydrogel pastes in different concentrations. The prepared alginate pastes with different PMO content were used to fabricate the step-gradient NC hydrogel with the aid of a 3D printing technique. The cell experiments demonstrated the PMO concentration-dependent cell migration towards the gradient hydrogel section that possessed a higher concentration of biopolymer-coated PMOs. Additionally, we demonstrated the potential application of our gradient NC hydrogel in migration and the subsequent enhanced osteogenic differentiation of human bone marrow derived mesenchymal stem cells (hBM MSC).

2. Materials and methods

2.1. Materials

PDL, hexadecyltrimethylammonium bromide (CTAB, 98%), 1,2-bis(trimethoxysilyl)ethane (BTME, 96%), *N*, *N*′-bis(2,6-dimethylphenyl)perylene-3,4,9,10-tetracarboxylic diimide (DXP), paraformaldehyde (PFA) and trypsin, were purchased from Sigma-Aldrich. Ethanol (absolute for analysis), ammonia solution (32%, pure) and hydrochloric acid (32%, for analysis), were purchased from Merck. Laponite powder was obtained from (Laponite RD) Kremer Pigmente GmbH & Co-KG, Germany. Trypan blue solution was purchased from Life Technologies GmbH. Phalloidine Alexa Fluor®488 was purchased from Invitrogen, and 4′,6-diamidino-2-phenylindole dihydrochloride (DAPI) was acquired from Polysciences Europe GmbH. The cell medium (RPMI 1640) supplemented with 10% (v/v) fetal bovine serum (FBS) was obtained from Biochrom, Germany.

2.2. General procedure for cell experiments in AlgL, $PMO^{0.3}$-AlgL, and $PMO^{0.9}$-AlgL homo scaffolds

The cells were carefully thawed and suspended in their specific medium (10% FBS + RPMI 1640). Then, the cells were seeded homogeneously onto the 3D printed homo AlgL, $PMO^{0.3}$-AlgL and $PMO^{0.9}$-AlgL scaffolds (approximately 20 000 cells for each scaffold). The scaffolds were covered with cell culture media (2 ml) and incubated for 10 min, 4 and 7 days at 37 °C and 5% CO_2. After the incubation periods, the scaffolds were washed twice with phosphate-buffered saline (PBS) to remove non-adhered cells. Subsequently, they were transferred to another cell culture plate and treated with EDTA (0.04% w/v in PBS, without Ca^{2+}/Mg^{2+}) with gentle mixing. The cells were counted immediately using a Neubauer chamber (trypan blue solution was used to detect dead cells).

2.3. General procedure for 3D printing of the step-gradient NC scaffolds (GradNCs)

AlgL, $PMO^{0.3}$-AlgL and $PMO^{0.9}$-AlgL (0.1 ml each) pastes were subsequently printed in a side-by-side orientation to form three connected hexagonal prisms (5 mm on each side and 2 mm in height) in the

horizontal (XY) plane. The final construct was cross-linked with a $CaCl_2$ (100 mM) solution, frozen at −20 °C for 16 h and then lyophilized with a freeze dryer for 16 h, giving rise to the GradNCs.

2.4. General procedure for the cell experiments in the 3D printed GradNC

The cells were carefully thawed and suspended in their specific medium (10% FBS + RPMI 1640). Then, the cells were seeded homogeneously onto each part of the GradNC (approximately 20 000 cells for each scaffold). The GradNC was covered with cell culture media (2 ml) and incubated for 10 min, 4 and 7 days at 37 °C and 5% CO_2. After the incubation periods, the scaffold was washed twice with PBS to remove non-adhered cells. Subsequently, the GradNC was separated into its parts (AlgL, $PMO^{0.3}$-AlgL and $PMO^{0.9}$-AlgL). These parts were transferred to another cell culture plate and treated with EDTA (0.04% w/v in PBS, without Ca^{2+}/Mg^{2+}) with gentle mixing. The cells were counted immediately using a Neubauer chamber (trypan blue solution was used to detect dead cells).

2.5. General procedure for cell migration experiments in the 3D printed GradNC

For the cell migration experiments, we used the above procedure, except here the cells were seeded homogeneously only onto the AlgL part of the GradNC (approximately 20 000 cells onto the hexagonal prism).

2.6. General procedure for the reverse cell migration experiments in the 3D printed GradNC

For the reverse cell migration experiments, we used the above procedure, except here the cells were seeded homogeneously only onto the $PMO^{0.9}$-AlgL part of the GradNC (approximately 20 000 cells on the hexagonal prism).

2.7. General procedure for hBM MSCs migration experiments in the 3D printed GradNC

The hBM MSCs were obtained from whole bone marrow (BM) cells (Lonza). They were cultured in alpha MEM (Sigma, St-Louis, MO, USA) supplemented with 20% FBS (Invitrogen), 1% penicillin and streptomycin (Sigma-Aldrich, St-Louis, MO, USA), and were incubated at 37 °C in a humidified atmosphere containing 5% CO_2 for 10 days and the culture medium was changed once every 2–3 days. At 80%–85% confluence, adherent hBM MSCs were trypsinized with TrypLE solution (Gibco Invitrogen), and cell viability was checked by trypan blue dye exclusion. In the present study, passage 3 (P3) hBM MSCs were seeded onto AlgL scaffolds and AlgL, $PMO^{0.3}$-AlgL, and $PMO^{0.9}$-AlgL scaffolds of the GradNC. Cell proliferation was evaluated with Presto Blue Staining solution and the optical density (OD) value was calculated depending on spectrophotometrical measurement.

2.8. Osteogenic differentiation capacity of hBM MSCs in the 3D printed GradNC

Osteogenic differentiation potentials of passage 3 hBM MSCs inside the printed construct (the hBM MSCs were seeded onto AlgL scaffolds and AlgL, $PMO^{0.3}$-AlgL and $PMO^{0.9}$-AlgL parts of GradNC) were analyzed by incubating them with and without osteogenic differentiation medium for 14 days. Osteogenic differentiation capacity was evaluated after Alizarin Red staining at days 7 and 14.

2.9. Characterization

The morphology of the AlgL, $PMO^{0.3}$-AlgL and $PMO^{0.9}$-AlgL scaffolds was investigated using a Zeiss 1540 EsB dual beam focused ion beam/field emission scanning electron microscope (SEM). The morphology of cells in hydrogels was determined using Brunel SP300-FL fluorescence microscopy. The silicon and magnesium ion-release analysis from nanoparticles and also from scaffolds were performed by Spectro ARCOS inductively coupled plasma optical emission spectroscopy (ICP-OES) from Spectro Analytical Instruments (Kleve, Germany). Tissue Scribe Gen. 3 (a 3D bio-printer by 3D Cultures) was used to print all scaffolds into computer-designed 3D structures. Anton Paar (Modular Compact Rheometer) was used for rheological analyses.

3. Results and discussion

We described the synthesis and characterization of PDL-coated PMOs previously [27]. Briefly, PMOs were loaded with DXP, a non-water-soluble fluorescent dye molecule (for detection of PMOs in hydrogels), and then coated with PDL. Polylysine, a biodegradable biopolymer, was used to coat surfaces to promote cell adhesion and growth [27, 28]. The PDL-coated PMOs were inserted into alginate (Alg)/Laponite hydrogel paste (AlgL) in different concentrations to generate PMO^{0}-AlgL = AlgL (pure Alg with 0 mg PMO/(1 ml paste)), $PMO^{0.3}$-AlgL (0.3 mg PMO/(1 ml paste)), and $PMO^{0.9}$-AlgL (0.9 mg PMO/(1 ml paste)). Laponite was used to improve the mechanical properties of alginate and thus to generate injectable paste for the 3D printer [29, 30]. The prepared AlgL pastes loaded with different concentrations of PMOs were first printed into 3D hexagonal prisms and cross-linked with a calcium source to obtain PMO^{x}-AlgL homo hydrogels (x = 0, 0.3, 0.9) (figures 1(A)–(C)). The $PMO^{0.3}$-AlgL as a representative example was also printed into different shapes (hexagon, cube, ear) to show the accuracy in shapes of the different structures in different sizes (figures 1(D)–(F)). Other alginate or Laponite-based scaffolds with good shape fidelity have been reported in the literature [31–33].

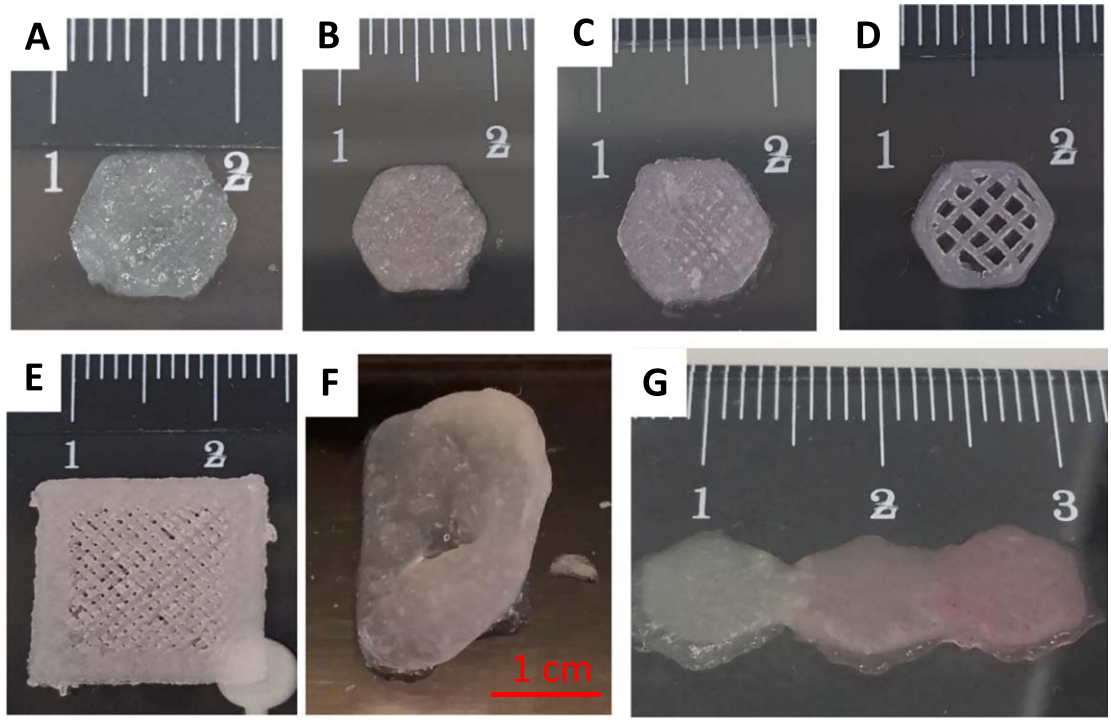

Figure 1. 3D printed NC homo hydrogels with different shapes. Hexagons of (A) AlgL, (B) $PMO^{0.3}$-AlgL and (C) $PMO^{0.9}$-AlgL. (D) A hexagon of $PMO^{0.3}$-AlgL with larger strand distance. (E) The cube shape of $PMO^{0.3}$-AlgL. (F) The ear shape of $PMO^{0.3}$-AlgL. (G) A gradient scaffold composed of AlgL, $PMO^{0.3}$-AlgL and $PMO^{0.9}$-AlgL.

Morphology, rheological, swelling, degradation and porosity properties of the prepared hydrogels were characterized using different techniques (figures S1, S2 are available online at stacks.iop.org/BF/11/045015/mmedia and tables S1–S4). The SEM images show the 3D porous AlgL hydrogel network, and the zoomed-in images show the PMOs embedded into the AlgL hydrogel wall (figure S1). Rheological measurements were performed to evaluate the effect of the amount of PMO on the mechanical properties of the AlgL hydrogel composition under shear stress. The results of rheological measurements indicated that a higher number of PMO particles led to the formation of more viscous gels than the pure alginate hydrogel itself. All pastes showed shear thinning effects at increasing shear rates. (figure S2(A)). Furthermore, the interactions between the PMOs and the AlgL resulted in slightly higher values of storage and loss modulus (figure S2(B)). The mechanical spectra were characterized by measurement of the storage modulus (G′), loss modulus (G″) and apparent viscosity as a function of angular frequency. The $PMO^{0.3}$-AlgL and $PMO^{0.9}$-AlgL displayed a higher storage modulus than loss modulus over the range of angular velocities. AlgL had almost the same storage and loss modulus until an angular velocity of ca. 1.0 s^{-1}. After this point, the paste showed elasticity. Our data suggested that PMO improved the shear thinning of AlgL and slightly enhanced the viscoeleastic properties of AlgL. Furthermore, we investigated the swelling ratio, the equilibrium water content (%), degradation behavior and porosity of the hydrogels (tables S1–S4). The 3D printed $PMO^{0.3}$-AlgL and $PMO^{0.9}$-AlgL hydrogels exhibited a higher swelling capacity, higher porosity and less degradation in comparison to the PMO-free AlgL hydrogel. The reason was attributed to the incorporation of hydrophilic porous PMOs into the hydrogel network that improves the hydrophilicity and mechanical stability of the network and increases water diffusion, while at the same time it decreases the degradation of the hydrogel. The weight losses (%) of the $PMO^{0.3}$-AlgL and $PMO^{0.9}$-AlgL hydrogels were less than AlgL in the presence of fibroblast cells showing the enhancement in the stability of AlgL with PMOs at 37 °C in the presence of cells for incubation times of 1 day, 4 and 7 days (table S3). Porosity measurements (table S4) showed that the 3D hydrogels with the PMOs had higher porosity than AlgL, because the PMOs enhanced the stability of the structure within the cross-linked hydrogel network.

The adhesive properties of the AlgL, $PMO^{0.3}$-AlgL and $PMO^{0.9}$-AlgL hydrogels were tested as well (for details see the supporting information (SI)) (figure S3(A), (B)). Adhesiveness is one of the desired properties of the engineered biomaterials. Such adhesives find applications in tissue engineering and surgery due to their ability to eliminate stress localization at the fractured surfaces, fast conjunction of fractures and ability to resist the separation of the rejoined fractions. We simulated the rejoining of an example of human femur fractions by using $PMO^{0.9}$-AlgL hydrogel (figures S3(C), (D)).

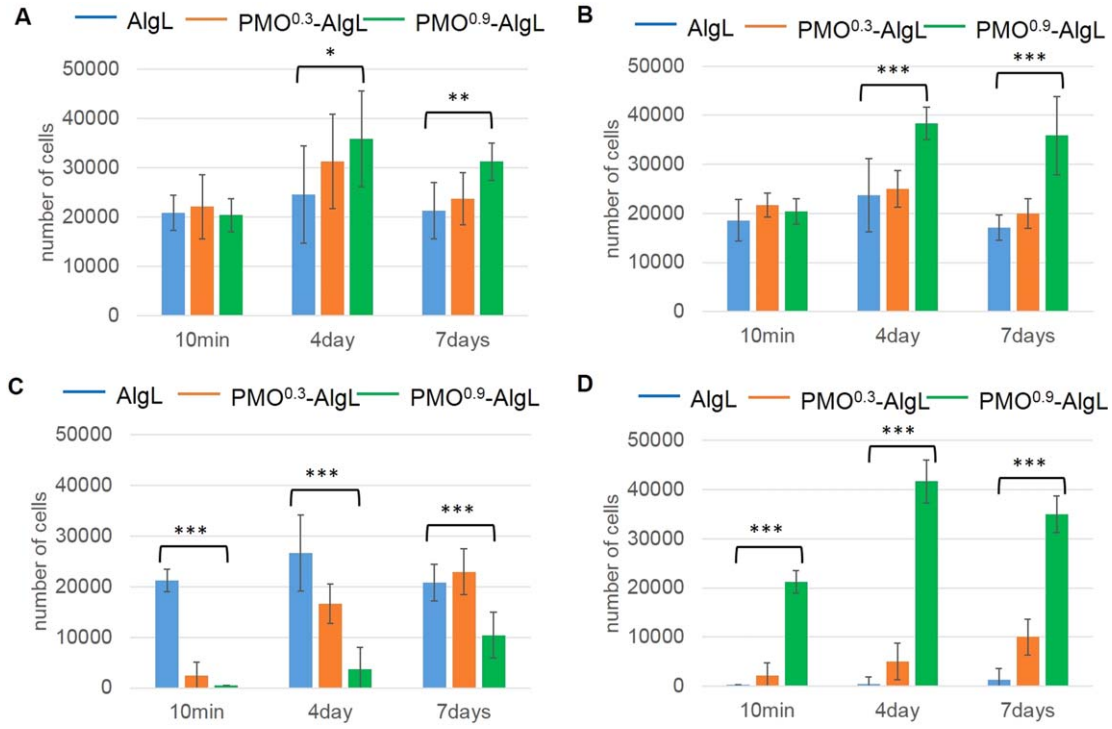

Figure 2. The number of fibroblast cells ($\times 10^3$) in AlgL, PMO$^{0.3}$-AlgL and PMO$^{0.9}$-AlgL homo scaffolds (A). The number of fibroblast cells ($\times 10^3$) in AlgL, PMO$^{0.3}$-AlgL and PMO$^{0.9}$-AlgL parts of the GradNC (B, C, D). Cells were added onto all parts of the GradNC (B). Cells were added only into the AlgL part of the GradNC (C). Cells were only added onto the PMO$^{0.9}$-AlgL part of the GradNC (D) ($N = 3$; data show significant differences; Anova: $p < 0.05$ with (*), $p < 0.01$ (**), $p < 0.001$ (***)).

Cell adhesion experiments were then carried out in freeze-dried 3D printed NC homo hydrogel scaffolds using first primary fibroblast cells (due to their importance in wound healing) [34] to determine whether the cells had different affinities for the hydrogels containing different concentrations of PMOs functionalized with the biopolymer. The cells were seeded onto AlgL, PMO$^{0.3}$-AlgL and PMO$^{0.9}$-AlgL and incubated for 10 min, 1 day and 7 days. After the incubation periods, the number of viable cells in each of the hydrogels was determined (figure 2(A), table S5). Our results show that cells had higher affinity to AlgL hydrogels loaded with the biopolymer-coated PMO particles than they did for PMO-free AlgL hydrogel (figure 2(A), table S5) (after 4 and 7 days). The alive cell numbers in AlgL hydrogels increased with the PMO concentration. The difference in the number of cells between the AlgL, PMO$^{0.3}$-AlgL and PMO$^{0.9}$-AlgL hydrogels became more pronounced after longer incubation time. We found 1.5 and 1.3 times more cells in PMO$^{0.9}$-AlgL hydrogel than AlgL and PMO$^{0.3}$-AlgL hydrogels (after 7 days of incubation), respectively, demonstrating enhanced cell adhesion with PMO concentration. It has been demonstrated by us [35, 36] and other groups [37, 38] that incorporation of NMs in hydrogel/hydrogel scaffolds and/or surfaces improves cell-material interaction due to an increase in the surface area of the material, and thus a higher number of binding sites for cell attachment.

Based on these observations we prepared step-gradient hydrogels to control the migration of cells by PMO concentration within the 3D network of hydrogel (figure 1(G)). The prepared AlgL, PMO$^{0.3}$-AlgL and PMO$^{0.9}$-AlgL pastes were printed in a side-by-side orientation, cross-linked and freeze-dried to form three connected hexagonal prism hydrogels where each hexagon contains different amounts of PMOs within the 3D hydrogel network. The final construction, freeze-dried GradNC was used for cell experiments to analyze the impact of PDL-coated PMO concentration on cell migration in a 3D network (figure 2(B), table S6). Almost the same numbers of cells were first seeded onto each hexagonal hydrogel of GradNC (figure S4(Ai)) and incubated for 10 min, 4 and 7 days as carried out for the homo hydrogels (for comparison approximately the same number of cells was seeded in each hexagon hydrogel as in the cell experiments for homo hydrogels described above). After the incubation periods, the GradNCs were separated into their parts (AlgL, PMO$^{0.3}$-AlgL and PMO$^{0.9}$-AlgL) (figure S4(Aii)). These parts were transferred to another cell culture plate, and the number of viable cells and cell viability in each separate part were determined. We observed an increase in the number of cells with PMO concentration, which became more pronounced at longer incubation times (figure 2(B), table S6). For example, we extracted 2 and 1.8 times more alive cells in PMO$^{0.9}$-AlgL hydrogel than AlgL and PMO$^{0.3}$-AlgL hydrogels, respectively, during 7

days of incubation, while the ratio between these hydrogels was 1.6 and 1.5 during 4 days of incubation. In addition, we determined a 75% increase in alive cell content in $PMO^{0.9}$-AlgL hydrogel from 10 min to 7 days of incubation, while AlgL and $PMO^{0.3}$-AlgL hydrogels showed an opposite trend (8% decrease in alive cell content in each hydrogel) within the same incubation period.

When we compared homo hydrogels (figure 2(A), table S5) and AlgL, $PMO^{0.3}$-AlgL and $PMO^{0.9}$-AlgL parts of GradNC (figure 2(B), table S6), we investigated significant differences in the live cell numbers. For example, after 7 days of incubation, the cell contents in the homo hydrogels, AlgL and $PMO^{0.3}$-AlgL were increased by 2% and 8%, respectively, while those in the AlgL and $PMO^{0.3}$-AlgL parts of the GradNC were decreased by 8%. On the other hand, the number of cells in the $PMO^{0.9}$-AlgL of homo hydrogel and GradNC showed 53% and 75% increase in the same incubation period. The smaller increase in the AlgL and $PMO^{0.3}$-AlgL and the higher increase in the $PMO^{0.9}$-AlgL parts of the GradNC than the respective homo hydrogels can be an indication of a movement of cells from the AlgL and $PMO^{0.3}$-AlgL towards the $PMO^{0.9}$-AlgL part of the GradNC.

Therefore, for better understanding, we performed additional cell experiments. We prepared a GradNC and seeded cells now only in the AlgL part of it (figure S4(B)). The final cell-laden GradNC was incubated for 10 min, 4 and 7 days. After incubation, we determined viable cell numbers in the AlgL, $PMO^{0.3}$-AlgL and $PMO^{0.9}$-AlgL parts of the GradNC (figure 2(C), table S7). After 10 min incubation period 90% of cells were obtained from AlgL and only 10% of cells were extracted from $PMO^{0.3}$-AlgL. However, with longer incubation times (4 and 7 days) we also extracted cells from the $PMO^{0.9}$-AlgL part of the GradNC. Furthermore, we observed a decrease in cell numbers in the AlgL, while there was a continuous increase in cell content in the $PMO^{0.3}$-AlgL part and $PMO^{0.9}$-AlgL parts of GradNC. These results were another sign of a migration of cells inside the GradNC matrix towards the higher concentration of PMOs.

In the next step we conducted reverse cell migration experiments. Cells were seeded into the $PMO^{0.9}$-AlgL part of the GradNC and incubated for the same periods as in the former experiments (figure S4(C)). The initial number of cells was 0, 9 and 91% in the AlgL, $PMO^{0.3}$-AlgL and $PMO^{0.9}$-AlgL parts of the GradNC, respectively (figure 2(D), table S8). We observed that the number of cells continuously increased in the $PMO^{0.3}$-AlgL part and that was first increased and then decreased in $PMO^{0.9}$-AlgL for the longer incubation time (7 days). Whereas we extracted few cells in AlgL only after 4 days of incubation, and the cell number was slightly increased during 7 days of incubation.

When we compare concentration-dependent cell migration (figure 2(C), table S7) and reverse cell migration experiments (figure 2(D), table S8), we investigated that cells migrated in both experiments towards the empty parts of the GradNC. However, the cell migration tendency was higher when cells were added in the AlgL part compared to the $PMO^{0.9}$-AlgL part of the GradNC. For example, if we make an approximate calculation, we found that the cell content in AlgL (1.3×10^3) after 7 days was 6% of the initial cell number (21.3×10^3) in the $PMO^{0.9}$-AlgL part of the GradNC (figure 2(D), table S8). On the other hand, the number of cells in $PMO^{0.9}$-AlgL (10.4×10^3) after the same incubation time was 49% of the cells which were seeded at the beginning into the AlgL (21.3×10^3) part of the GradNC confirming the PMO concentration-dependent cell migration (figure 2(C), table S7).

Cell experiments were also monitored by fluorescence microscopy (figures S5–S7). The membrane and the nucleus of the cells were co-stained with Phalloidine Alexa Fluor® 488 (green) and 4′,6-diamidino-2-phenylindole-6-carboxamidine (DAPI, blue), respectively (see the SI). The fluorescence microscopy images confirm the PMO concentration-dependent cell migration within the 3D network of the GradNC. In addition, SEM images (figure S8) of cells in the respective hydrogels showed the adhered cells inside the hydrogel scaffold network.

The migration rate of cells on the substrate surface is influenced by the type and density of adhesive ligands on substrate surfaces. Cell migration requires an optimum strength of interaction of cells with a substrate that should be sufficient for cell adhesion but should not be so strong that it prevents the detachment of cells. Many studies used integrin binding ligands, such as the arginine-glycine-aspartic acid (RGD) peptide sequence which is present in fibronectin and other matrix proteins [39], to promote cell adhesion and migration [40]. Moreover, polylysine has been widely used as a cell adhesive polymer to enhance cell attachment to untreated substrate surfaces. Positively charged polylysine binds electrostatically to the negatively charged cells, thus improving cell adhesion on substrate surfaces. Recently, it has been shown by Vig *et al* that cells on polylysine-coated surfaces move faster than cells on fibronectin-coated surfaces when the cells move collectively [41]. This result was attributed to the collective cell migration that resulted in higher intracellular contractile forces that push the cell across the substrate. Besides cell adhesive ligands, nanoparticle density and surface roughness on substrates are other important factors for cell adhesion, spreading and migration [35, 37, 42] due to an increase in the surface area of the substrate surface. The studies showed that at optimum value of the nanoparticle and adhesive ligand density, cells found the best conditions for adhesion and migration. Therefore, we suggest that our observed cell adhesion and migration results are

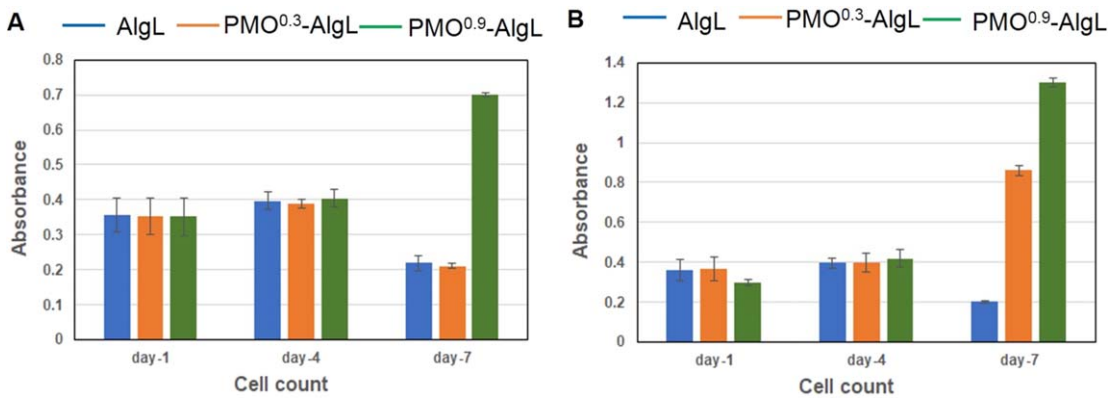

Figure 3. The OD number of hBM MSCs in AlgL, PMO$^{0.3}$-AlgL and PMO$^{0.9}$-AlgL homo scaffolds. Cells were added only into the AlgL part of the GradNC (A). Cells were added onto all parts of the GradNC (B). (The number of repeated experiments N = 3).

mediated by the presence of both PDL and PMOs in the network of the PMO-AlgL.

After we demonstrated the migration of fibroblasts in GradNC, we performed cell experiments using hBM MSCs to show potential applications of our step-gradient NC hydrogel. Recent studies have shown that the composite films of graphene oxide (GO) and poly-lysine [43] and hyaluronic acid/poly-*L*-lysine bilayered silica nanoparticles [44] can support the growth of MSCs with a high proliferation rate, and accelerate the osteogenic differentiation of MSCs. In addition, silica-based NMs are of particular interest for bone tissue regeneration due to the mechanical and biocompatibile properties (presenting osteoconductive and osteoinductive properties) of silica and derivatives such as bioactive glass. Silica-based NMs have been demonstrated to promote differentiation of bone forming osteoblasts [45–48]. Therefore, we investigated the PDL-coated silica-based PMO-mediated hBM MSC migration and osteogenic differentiation in the 3D network of the GradNC. The hBM MSCs were seeded onto the AlgL, PMO$^{0.3}$-AlgL and PMO$^{0.9}$-AlgL parts of the GradNC, and then incubated for 7 days. After the incubation periods, the number of viable cells in each of the hydrogels was determined. For this purpose, the GradNCs were separated into their parts (AlgL, PMO$^{0.3}$-AlgL and PMO$^{0.9}$-AlgL). These parts were transferred to another cell culture plate, and cell proliferation in each separate part was determined. We investigated that cells migrated towards the PMO$^{0.9}$-AlgL part of the GradNC (figures 3(A) and (B)). It has been shown in figure 3(A) that when the cells were added on AlgL, cells migrated towards the empty gradients during 7 days of culture and increased their numbers in PMO$^{0.9}$-AlgL at day 7. We found that the cell content in PMO$^{0.9}$-AlgL after 7 days of culture was two-fold higher compared to the first day cell number. Similarly, a high number of cells was found in PMO$^{0.9}$-AlgL compared to AlgL hydrogels (3.2-fold) at day 7. On the other hand, when hBM MSCs were added in the same amount on all parts of the GradNC at the initial step, the cells showed a similar migration and expansion profile when they were added to the AlgL alone experiments. We found that the cell content in PMO$^{0.9}$-AlgL after 7 days was 4.4-fold compared to the first day cell numbers and 6.4-fold compared to AlgL cell numbers at day 7 (figure 3(B)).

It has been published that the use of many ECM-derived biomaterials, including gelatin, collagen and hyaluronic acid, are limited due to the lack of osteogenic factors or other ions which could enhance mineralization. To mimic the chemical composition of natural bone, some biomimetic inorganic particles, such as hydroxyapatite, silicate, ceramic hydrogel and a titanium compound, are commonly applied within hydrogels. Based on this concept, we added our system Laponite (nanosilicate) and PMOs to obtain bone biomimetic surfaces. Thus, we tested hBM MSC embedded Laponite/PMO-based 3D printed hydrogels for osteogenic differentiation.

Osteogenic differentiation potentials of passage 3 hBM MSCs inside the printed construct (the hBM MSCs were seeded only onto AlgL or onto all parts of the AlgL, PMO$^{0.3}$-AlgL and PMO$^{0.9}$-AlgL of the GradNC) were analyzed by incubating them with and without osteogenic differentiation medium for 7 and 14 days. Osteogenic differentiation capacity and the quantitative amount of Ca^{2+} deposition in GradNCs were evaluated by Alizarin Red staining (figure 4) and using a QuantiChrom Calcium Assay Kit (figure S9), respectively. After Alizarin Red staining at days 7 and 14, we observed Ca^{2+} deposition in the GradNC in the presence and also even in the absence of osteogenic medium. Furthermore, when we seeded cells into the AlgL part of the GradNC, we observed an increase in Ca^{2+} deposition in the PMO$^{0.3}$-AlgL and PMO$^{0.9}$-AlgL parts of the GradNC due to the migration capacity of cells towards PMO$^{0.9}$-AlgL in both culture days and conditions (figures S9(B), (D)). In addition, osteogenic differentiation was determined through the bone-related proteins, osteopontin (OPN) and osteocalcin (OCN). OCN and OPN, non-

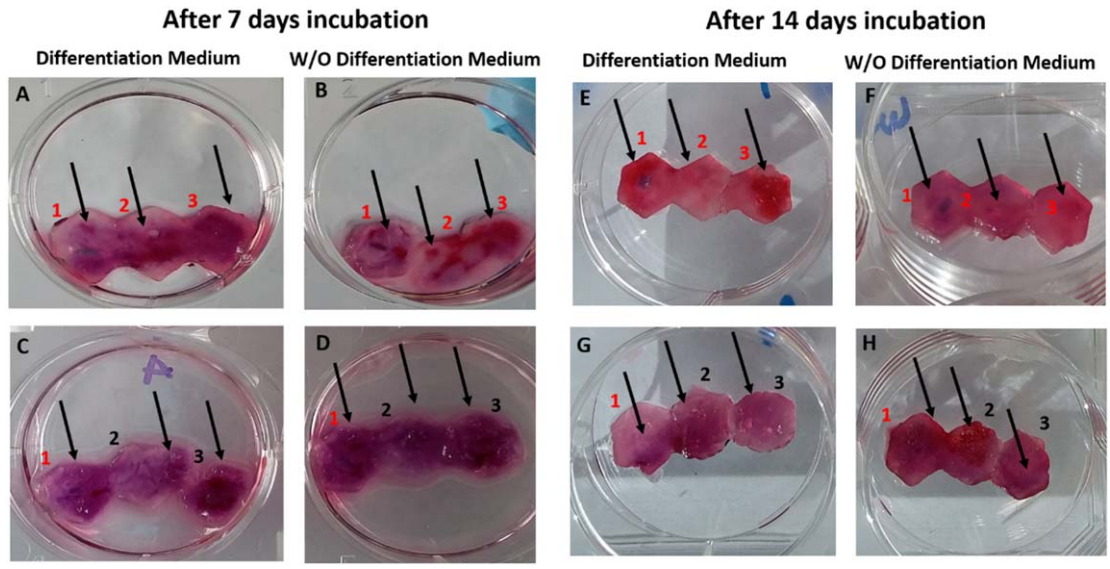

Figure 4. Mineralization analysis of hBM MSCs in GradNC after 7 (A)–(D) and 14 (E)–(H) days of culturing in osteogenic (differentiation) and alpha MEM medium (w/o differentiation) using Alizarin Red staining (shown by black arrows). Cells were added onto all parts of the GradNC ((A), (B), (E), (F)). Cells were added only into the AlgL part of the GradNC ((C), (D), (G), (H)). 1: AlgL, 2: $PMO^{0.3}$-Alg, 3: $PMO^{0.9}$-Alg.

collagenous proteins, are structural elements of bone ECM and are involved in the biological and mechanical functions of bone. The OPN (at day 7) (figure S10) and osteocalcin (OCN) (at day 14) (figure S11) levels were evaluated by immunofluorescence staining. In all of the sections of GradNC examined, we found higher OPN and OCN levels in the presence of differentiation medium than in the absence of differentiation medium. More importantly, we observed an increase in the OPN and OCN level towards the $PMO^{0.3}$-AlgL and $PMO^{0.9}$-AlgL parts of the GradNC. This result is more pronounced in the presence of differentiation medium. Thus, ECM protein synthesis confirmed nanoparticle-dependent migration and subsequent osteogenic differentiation of hBM MSCs in our 3D printed gradient construction.

Recently, the effect of nanosilicates and other silica-based materials on hMSCs was evaluated by different groups [49–55]. It has been reported that released minerals from nanosilicates and other silica-based materials regulate the proliferation and osteogenic differentiation of stem cells. Just as silicon ions mediate stem cell differentiation by triggering cWnt signaling pathways, magnesium ions up-regulate the production of collagen and vascular endothelial growth factor (VEGF) in hMSCs and enhance osteogenic activity, and lithium stimulates Wnt-responsive genes by increasing cytoplasmic β-catenin and improves bone formation and bone mass [49–55]. Furthermore, a transcriptomic profile of hMSCs in response to nanosilicate exposure was investigated. The interaction of nanosilicates with the cell membrane induced surface receptors, and resulted in widespread changes in gene expression from a variety of pathways, including the stress-responsive and surface-receptor-mediated MAPK/ERK pathways. Similarly, the data indicated that internalization of nanosilicates and subsequent release of mineral ions mediated biochemical signaling that stimulated osteochondral differentiation of hMSCs [49]. In this respect, we performed ion-release experiments (figures S12–S15, tables S9–S12). Silicon and magnesium ion-release analysis from nanoparticles and hydrogel scaffolds were carried out by ICP-OES measurements. We first measured the diffused ions out of AlgL, $PMO^{0.3}$-AlgL and $PMO^{0.9}$-AlgL (figures S12, S13, tables S9, S10). Two bioactive ions (silicon ions and magnesium ions) that can promote osteogenesis were measured [56, 57]. The ICP-OES results demonstrated that the amount of diffused Si^{4+} und Mg^{2+} was higher in PMO-loaded AlgL than AlgL itself at 1 day incubation time. On the other hand, the opposite trend was observed at 14 days of incubation. We observed a decrease in the number of diffused ions with increasing PMO concentration within the AlgL network. This indicates that a higher PMO concentration may cause higher cross-linking density that hindered the diffusion of ions from the respective scaffolds. This result is complementary with the degradation behavior of AlgL, $PMO^{0.3}$-AlgL and $PMO^{0.9}$-AlgL (table S3). Thereafter, we measured the released amount of Si^{4+} and Mg^{2+} from Laponite and Si^{4+} from PMO to support our results (figures S14, S15, tables S11, S12). We tested the same amount of Laponite and PMO concentrations that we used in AlgL, $PMO^{0.3}$-AlgL and $PMO^{0.9}$-AlgL. The first concentration consisted of Laponite (L), the second concentration was composed of Laponite + $PMO^{0,3}$ ($PMO^{0,3}$-L) and the third concentration contained Laponite + $PMO^{0,9}$ ($PMO^{0,9}$-L). The ICP results showed that Si^{4+} und Mg^{2+} were released from PMO and Laponite gradually. The released amount of Si^{4+} was higher in $PMO^{0,3}$-L and $PMO^{0,9}$-L than sample L due to the presence of PMO. In addition, the released amount of Mg^{2+}

from all samples is the same because only Laponite contains Mg^{2+} ions (table S12 and figure S15). These results indicate the impact of PMO and its concentration on the osteogenic differentiation of hBM MSCs inside the GradNC.

4. Conclusions

In this contribution, we reported the 3D printing of a step-gradient NC hydrogel and its application in cell migration studies. The cell experiments demonstrated that cells had higher affinity for PMO-incorporated AlgL hydrogels than PMO-free AlgL, and showed enhanced cell growth in higher concentrations of PMOs. We utilized the PMO concentration-dependent cell preference to direct cell migration towards the GradNC section that possessed a higher concentration of biopolymer-coated PMOs. The PMO-based hydrogels facilitated migration and osteogenic differentiation of hBM MSCs. The extracellular matrix protein synthesis by differentiated cells inside the hydrogels, Ca^{2+} deposition and ion-release experiments confirmed these results. In addition, our NC hydrogels display self-adhesive properties indicating the potential application of this biomaterial as tissue adhesives. Overall, we believe that the strategy of incorporating bioactive silica-based NMs into alginate as printing agents will be promising for bone tissue engineering. In the long term, we propose that such NC hydrogels with gradient properties and specific functional groups on the surface of NMs, generated easily by 3D printing technology, should be used in bioengineering for the construction of new biomaterials for wound healing, regenerative medicine and tissue engineering applications.

Acknowledgments

We thank Deutsche Forschungsgemeinschaft for funding, Dr Celeste Riley Brennecka for scientific editing and Pooya Dorri for his technical assistance. Nihal Ermis thanks the European Union Erasmus Scholarship.

ORCID iDs

Ali Khademhosseini https://orcid.org/0000-0001-6322-8852
Nermin Seda Kehr https://orcid.org/0000-0003-2275-1254

References

[1] Girard P P, Cavalcanti-Adam E A, Kemkemer R and Spatz J P 2007 Cellular chemomechanics at interfaces: sensing, integration and response *Soft Matter* **3** 307–26
[2] Khademhosseini A, Langer R, Borenstein J and Vacanti J P 2006 Microscale technologies for tissue engineering and biology *Proc. Natl Acad. Sci. USA* **103** 2480–7
[3] Langer R and Vacanti J P 1993 Tissue engineering *Science* **260** 920–6
[4] Khademhosseini A, Vacanti J P and Langer R 2009 Tissue engineering *Sci. Am.* **300** 64–71
[5] Sharma R I and Snedeker J G 2010 Biochemical and biomechanical gradients for directed bone marrow stromal cell differentiation toward tendon and bone *Biomaterials* **31** 7695–704
[6] Veevers-Lowe J, Ball S G, Shuttleworth A and Kielty C M 2011 Mesenchymal stem cell migration is regulated by fibronectin through $\alpha5\beta1$-integrin-mediated activation of PDGFR-β and potentiation of growth factor signals *J. Cell Sci.* **124** 1288–300
[7] Hadden W J *et al* 2017 Stem cell migration and mechanotransduction on linear stiffness gradient hydrogels *PNAS* **114** 5647–52
[8] de Lucas B, Perez L M and Galvez B G 2018 Importance and regulation of adult stem cell migration *J. Cell. Mol. Med.* **22** 746–54
[9] Bracaglia L G, Smith B T, Watson E, Arumugasaamy N, Mikos A G and Fisher J P 2017 3D printing for the design and fabrication of polymer-based gradient scaffolds *Acta Biomater.* **56** 3–13
[10] Luca A D, Blitterswijk C V and Moroni L 2015 The osteochondral interface as a gradient tissue: from development to the fabrication of gradient scaffolds for regenerative medicine *Birth Defects Res.* **105** 34–52
[11] Melchels F P, Feijen J and Grijpma D W 2010 A review on stereolithography and its applications in biomedical engineering *Biomaterials* **31** 6121–30
[12] Chimene D, Peak C W, Gentry J L and James K C 2018 Nanoengineered ionic–covalent entanglement (NICE) bioinks for 3D bioprinting *ACS Appl. Mater. Interfaces* **10** 9957–68
[13] Luca A D, Longoni A, Criscenti G, Moldero I L, Gunnewiek M K, Vancso J, Blitterswijk C, Mota C and Moroni L 2016 Surface energy and stiffness discrete gradients in additive manufactured scaffolds for osteochondral regeneration *Biofabrication* **8** 015014
[14] Gurkan U A, Assal R E, Yildiz S E, Sung Y, Trachtenberg A J, Kuo W P and Demirci U 2014 Engineering anisotropic biomimetic fibrocartilage microenvironment by bioprinting mesenchymal stem cells in nanoliter gel droplets *Mol. Pharmaceutics* **11** 2151–9
[15] Byambaa B, Annabi N, Yue K, Trujillo-de Santiago G, Alvarez M M, Jia W, Kazemzadeh-Narbat M, Shin S R, Tamayol A and Khademhosseini A 2017 Bioprinted osteogenic and vasculogenic patterns for engineering 3D bone tissue *Adv. Healthc. Mater.* **6** 1700015
[16] Cross L M, Shah K, Palani S, Peak C W and Gaharwar A K 2018 Gradient nanocomposite hydrogels for interface tissue engineering *Nanomedicine.* **14** 2465–74
[17] Gaharwar A K, Peppas N A and Khademhosseini A 2014 Nanocomposite hydrogels for biomedical applications *Biotechnol. Bioeng.* **111** 441–53
[18] Wang Q, Mynar J L, Yoshida M, Lee E, Lee M, Okuro K, Kinbara K and Aida T 2010 High-water-content mouldable hydrogels by mixing clay and a dendritic molecular binder *Nature* **463** 339–43
[19] Fattahi P, Dover J T and Brown J L 2017 3D near-field electrospinning of biomaterial microfibers with potential for blended microfiber-cell-loaded gel composite structures *Adv. Healthc. Mater.* **6** 1700456
[20] Billiet T, Vandenhaute M, Schelfhout J, Van Vlierberghe S and Dubruel P A 2012 A review of trends and limitations in hydrogel-rapid prototyping for tissue engineering *Biomaterials* **33** 6020–41
[21] Motealleh A and Kehr N S 2017 Nanocomposite hydrogels and their applications in tissue engineering *Adv. Healthc. Mater* **6** 16009388
[22] Mannoor M S, Jiang Z, James T, Kong Y L, Malatesta K A, Soboyejo W O, Verma N, Gracias D H and McAlpine M C 2013 3D printed bionic ears *Nano Lett.* **13** 2634–9
[23] Castro N J, Patel R and Zhang L G 2015 Nanopatterned human iPSC-based model of a dystrophin-null cardiomyopathic phenotype *Cel. Mol. Bioeng.* **8** 416–32

[24] Gou M, Qu X, Zhu W, Xiang M, Yang J, Zhang K, Wie Y and Chen S 2014 Bio-inspired detoxification using 3D-printed hydrogel nanocomposites *Nat. Commun.* **5** 3774
[25] Chimene D, Peak C W, Gentry J L, Carrow J K, Cross L M, Mondragon E, Cardoso G B, Kaunas R and Gaharwar A K 2018 Nanoengineered ionic−covalent entanglement (NICE) bioinks for 3D bioprinting *ACS Appl. Mater. Interfaces* **10** 9957–68
[26] Wilson S A, Cross L M, Peak C W and Gaharwar A K 2017 Shear-thinning and thermo-reversible nanoengineered inks for 3D bioprinting *ACS Appl. Mater. Interfaces* **9** 43449–58
[27] Motealleh A and Kehr N S 2017 Janus nanocomposite hydrogels for chirality-dependent cell adhesion and migration *ACS Appl. Mater. Interfaces* **9** 33674–82
[28] Kehr N S and Jose J 2017 Chirality-dependent cellular uptake of chiral nanocarriers and intracellular delivery of different amounts of guest molecules *Appl. Surf. Sci.* **425** 432–9
[29] Li Y, Maciel D, Tomás H, Rodrigues J and MaHand S X 2011 pH sensitive laponite/alginate hybrid hydrogels: swelling behavior and release mechanism *Soft Matter.* **7** 6231–8
[30] Ahlfeld T, Cidonio G, Kilian D, Duin S, Akkineni A R, Dawson J I, Yang S M, Lode A, Oreffo R O C and Gelinsky M 2017 Development of a clay based bioink for 3D cell printing for skeletal application *Biofabrication* **9** 034103
[31] Gao Q *et al* 2019 3D printing of complex GelMA-based scaffolds with nanoclay *Biofabrication* **11** 035006
[32] Lin Z, Wu M, He H, Liang Q, Hu C, Zeng Z, Cheng D, Wang G and Chen D 2019 3D printing of mechanically stable calcium-free alginate-based scaffolds with tunable surface charge to enable cell adhesion and facile biofunctionalization *Adv. Funct. Mater.* **29** 1808439
[33] Hong S, Sycks D, Chan H F, Lin S, Lopez G P, Guilak F, Leong K W and Zhao X 2015 3D printing of highly stretchable and tough hydrogels into complex, cellularized structures *Adv. Mater.* **27** 4035–40
[34] Bainbridge P 2013 Wound healing and the role of fibroblasts *J. Wound Care* **22** 407–8
[35] Kehr N S, Motealleh A and Schäfer A H 2016 Cell growth on 'Janus' density gradients of bifunctional zeolites L *ACS Appl. Mater. Interfaces* **8** 35081–90
[36] Kehr N S, Atay S and Ergün B 2015 Self-assembled monolayers and nanocomposite hydrogels of functional nanomaterials for tissue engineering applications *Macromol. Biosci.* **15** 445–63
[37] Arnold M *et al* 2008 Induction of cell polarization and migration by a gradient of nanoscale variations in adhesive ligand spacing *Nano Lett.* **8** 2063–9
[38] Cousins B G, Allison H E, Doherty P J, Edwards C, Garvey M J, Martin D S and Williams R L 2007 Effects of a nanoparticulate silica substrate on cell attachment of candida albicans *J. Appl. Microbiol.* **102** 757–65
[39] Ruoslahti E 1996 RGD and other recognition sequences for integrins *Annu. Rev. Cell Dev. Biol.* **12** 697–715
[40] Stupack D G and Cheresh D A 2002 ECM remodeling regulates angiogenesis: endothelial integrins look for new ligands *Science Signalling* **2002** pe7
[41] Vig D K, Hamby A E and Wolgemuth C W 2017 Cellular contraction can drive rapid epithelial flows *Biophys. J.* **113** 1613–22
[42] Kunzler T P, Drobek T, Schuler M and Spencer N D 2007 Systematic study of osteoblast and fibroblast response to roughness by means of surface-morphology gradients *Biomaterials* **28** 2175–82
[43] Qi W, Yuan W, Yan J and Wang H 2014 Layer-by-layer assembled graphene oxide composite films for enhanced mechanical properties and fibroblast cell affinity *J. Mater. Chem.* B **2** 5461
[44] Amorim S, Martins A, Neves N M, Reisab R L and Pires R A 2014 Hyaluronic acid/poly-L-lysine bilayered silica nanoparticles enhance the osteogenic differentiation of human mesenchymal stem cells *J. Mater. Chem.* B **40** 6939–46
[45] Ha S W, Weitzmann M N and Beck G R Jr 2014 Bioactive silica nanoparticles promote osteoblast differentiation through stimulation of autophagy and direct association with LC3 and p62 *ACS Nano* **8** 5898–910
[46] Beck G R Jr, Ha S W, Camalier C E, Yamaguchi M, Li Y, Lee J K and Weitzmann M 2010 Bioactive silica based nanoparticles stimulate bone forming osteoblasts, suppress bone esorbing osteoclasts, and enhance bone mineral density *in vivo Nanomedicine* **8** 793–803
[47] Weitzmann M N, Ha S W, Vikulina T, Roser-Page S, Lee J K and Beck G R Jr 2015 Bioactive silica nanoparticles reverse age-associated bone loss in mice *Nanomedicine* **11** 959–67
[48] Ha S W, Viggeswarapu M, Habib M M and Beck G R Jr 2018 Bioactive effects of silica nanoparticles on bone cells are size, surface, and composition dependent *Acta Biomater.* **82** 184–6
[49] Carrow J K, Cross L M, Reese R W, Jaiswal M K, Gregory C A, Kaunas R, Singh I and Gaharwar A K 2018 Widespread changes in transcriptome profile of human mesenchymal stem cells induced by two-dimensional nanosilicates *Proc. Natl Acad. Sci. USA* **115** E3905–13
[50] Han P, Wu C and Xiao Y 2013 The effect of silicate ions on proliferation, osteogenic differentiation and cell signalling pathways (WNT and SHH) of bone marrow stromal cells *Biomater Sci* **1** 379–92
[51] Yoshizawa S, Brown A, Barchowsky A and Sfeir C 2014 Magnesium ion stimulation of bone marrow stromal cells enhances osteogenic activity, simulating the effect of magnesium alloy degradation *Acta Biomater.* **10** 2834–42
[52] Clément-Lacroix P, Ai M, Morvan F, Roman-Roman S, Vayssière B, Belleville C, Estrera K, Warman M L, Baron R and Rawadi G 2005 Lrp5-independent activation of Wnt signaling by lithium chloride increases bone formation and bone mass in mice *PNAS* **102** 17406–11
[53] Zhai X, Ma Y, Hou C, Gao F, Zhang Y, Ruan C, Pan H, Lu W W and Liu W 2017 3D-printed high strength bioactive supramolecular polymer/clay nanocomposite hydrogel scaffold for bone regeneration *ACS Biomater. Sci. Eng.* **3** 1109–18
[54] Xavier J R, Thakur T, Desai P, Jaiswal M K, Sears N, Cosgriff-Hernandez E, Kaunas R and Gaharwar A K 2015 Bioactive nanoengineered hydrogels for bone tissue engineering: a growth-factor-free approach *ACS Nano* 9 **3** 3109–18
[55] Feng C, Deng Z C, Li G, Chang J, Zhang Z, Jiang X and Wu C 2017 3D printing of lotus root-like biomimetic materials for cell delivery and tissue regeneration *Adv. Sci.* **4** 1700401
[56] Wong H M, Wu S, Chu P K, Cheng S H, Luk K D, Cheung K M and Yeung K W 2013 Low-modulus Mg/PCL hybrid bone substitute for osteoporotic fracture fixation *Biomaterials* **34** 7016–32
[57] Reffitt D M, Ogston N, Jugdaohsingh R, Cheung H F J, Evans B A J, Thompson R P H, Powell J J and Hampson G N 2003 Orthosilicic acid stimulates collagen type 1 synthesis and osteoblastic differentiation in human osteoblast-like cells *in vitro Bone* **32** 127–35